

# Pressure-driven superconductivity in the transition-metal pentatelluride $\text{HfTe}_5$

Yanpeng Qi,<sup>1</sup> Wujun Shi,<sup>1,2</sup> Pavel G. Naumov,<sup>1</sup> Nitesh Kumar,<sup>1</sup> Walter Schnelle,<sup>1</sup> Oleg Barkalov,<sup>1</sup> Chandra Shekhar,<sup>1</sup> Horst Borrmann,<sup>1</sup> Claudia Felser,<sup>1</sup> Binghai Yan,<sup>1,2,3,\*</sup> and Sergey A. Medvedev<sup>1,†</sup>

<sup>1</sup>Max Planck Institute for Chemical Physics of Solids, 01187 Dresden, Germany

<sup>2</sup>School of Physical Science and Technology, ShanghaiTech University, Shanghai 200031, China

<sup>3</sup>Max Planck Institute for the Physics of Complex Systems, 01187 Dresden, Germany

(Received 14 March 2016; revised manuscript received 13 June 2016; published 24 August 2016)

The discovery of superconductivity in hafnium pentatelluride  $\text{HfTe}_5$  under high pressure is reported. Two structural phase transitions and metallization with superconductivity developing at around 5 GPa are observed. A maximal critical temperature of 4.8 K is attained at a pressure of 20 GPa, and superconductivity persists up to the maximum pressure of the study (42 GPa). The combination of electrical transport and crystal structure measurements as well as theoretical electronic structure calculations enables the construction of a phase diagram of  $\text{HfTe}_5$  under high pressure.

DOI: 10.1103/PhysRevB.94.054517

## I. INTRODUCTION

The layered transition-metal chalcogenides,  $MX_n$  ( $M$  is a transition metal;  $X$  is a chalcogen element S, Se, Te;  $n = 2, 3, 5$ ), have been intensively studied for their rich physics. Decades ago, a large choice of such compounds has been synthesized and investigated, chiefly for their structural and electrical transport properties [1–3]. Among these materials, owing to the high atomic weight and the strong spin-orbit coupling, the tellurides are of specific importance.

The interest in this class of compounds has recently been rekindled by the observation of extremely large magnetoresistance in ditellurides such as  $\text{WTe}_2$  and  $\text{MoTe}_2$  [4,5]. They have been predicted to be Weyl semimetals [6,7] and quantum spin Hall insulators [8] in bulk and monolayer form, respectively, and thus have promising potential applications in electronics and spintronics [9,10]. Tritellurides, typified by  $\text{ZrTe}_3$ , often present a Peierls instability and a charge density wave (CDW) transition at low temperature [11]. Moreover, bulk superconductivity (SC) emerges upon suppression of CDW order in  $\text{ZrTe}_3$  [12]. Pentatellurides  $M\text{Te}_5$  ( $M = \text{Zr}$  or  $\text{Hf}$ ) are the highest tellurides in  $M\text{Te}_n$ . Particularly, a number of  $M\text{Te}_5$  compounds have been previously investigated for the enigmatic resistivity anomaly [13–15], thermoelectric properties [16], and quantum oscillations [17,18]. Recently, *ab-initio* calculations indicated that single-layer  $M\text{Te}_5$  compounds may be large-gap quantum spin Hall insulators [19]. In contrast, recent experiments with angle-resolved photoemission spectroscopy suggested  $\text{ZrTe}_5$  to be a three-dimensional (3D) Dirac semimetal [20]. Moreover, a chiral magnetic effect associated with the transformation from a Dirac semimetal to a Weyl semimetal was observed on  $\text{ZrTe}_5$  in magneto-transport measurement [20,21].  $M\text{Te}_5$  compounds were predicted to be located close to the phase boundary between the weak and strong topological insulators and to provide a platform to study topological quantum-phase transitions [19].

As a powerful tool to tune the electronic properties, pressure was also applied to these compounds. Recently,

a pressure-induced semimetal to superconductor transition was observed in  $\text{ZrTe}_5$  [22], while the behavior of the related  $\text{HfTe}_5$  under pressure is yet to be explored. In the present paper, we investigate the above mentioned issues for hafnium pentatelluride  $\text{HfTe}_5$ . Through electrical transport and Raman scattering measurements, we find SC in two high-pressure phases of  $\text{HfTe}_5$  with different normal-state features. Often SC emerges in transition-metal chalcogenides when a resistivity maximum or CDW transition is suppressed by applied pressure. This seems to be also the case for  $\text{HfTe}_5$ : SC appears at a pressure of 5 GPa, exhibits a maximal critical temperature ( $T_c$ ) of 4.8 K at 20 GPa, and persists till the highest measured pressure of 42 GPa. The recent successes of high-pressure studies on  $MX_n$  materials demonstrate their unique potential for uncovering novel physical properties in topological materials.

## II. EXPERIMENTAL AND COMPUTATIONAL DETAILS

Single crystals of  $\text{HfTe}_5$  were prepared by a flux-growth method using Te as self-flux. In a typical synthesis, pieces of Hf and a large excess of Te as flux were weighed in a ratio  $\text{Hf}_{0.0025}\text{Te}_{99.9975}$  and transferred to an alumina crucible inside an argon filled glove box. The crucible was then sealed inside a quartz tube under vacuum. The mixture was heated first to 900 °C for a day followed by rapid cooling to 580 °C. At this temperature further slow cooling with a rate of 0.5 K h<sup>-1</sup> was employed until 470 °C, where the excess of Te was decanted. Elemental compositions were determined using energy-dispersive x-ray spectroscopy (EDXS). The micrometer-scale compositions within the main phase were probed at 5–10 spots, and the results were averaged. The structures of the  $\text{HfTe}_5$  crystals were investigated using single-crystal x-ray diffraction (SXRD) with Mo  $K_{\alpha}$  radiation.

The electrical resistivity  $\rho$  was measured using a four-probe method (low-frequency alternating current, Physical Property Measurement System [PPMS], Quantum Design), and the heat capacity was determined by a relaxation method (HC option, PPMS, Quantum Design).

High-pressure resistivity and Raman spectroscopy measurements up to 42 GPa were performed in a nonmagnetic

\*Binghai.Yan@cpfs.mpg.de

†Sergiy.Medvedev@cpfs.mpg.de

diamond anvil cell equipped with diamond anvils with  $500\text{ }\mu\text{m}$  culets [23,24]. A cubic BN/epoxy mixture was used for the insulation of the sample against the metallic tungsten gasket, and  $5\text{ }\mu\text{m}$  thick Pt foil was employed for the electrical leads. The sample was loaded without pressure transmitting medium into the sample chamber of  $200\text{ }\mu\text{m}$  diameter with thickness  $\approx 40\text{ }\mu\text{m}$ . Resistivity was measured in the temperature range  $1.5$ – $300\text{ K}$  by a direct-current van der Pauw technique. Pressure was determined using the ruby scale for small chips of ruby placed in contact with the sample [25]. The high-pressure Raman spectra were recorded using a customary micro-Raman spectrometer with a HeNe laser as the excitation source and a single-grating spectrograph with  $1\text{ cm}^{-1}$  resolution.

Density-functional theory (DFT) calculations were performed using the Vienna *Ab initio* Simulation Package (VASP) with plane-wave basis [26]. The interactions between the valence electrons and ion cores were described by the projector augmented wave method [27,28]. The exchange and correlation energy was formulated by the generalized gradient approximation with the Perdew-Burke-Ernzerhof scheme [29]. Van der Waals corrections were also included via a pairwise force field of the Grimme method [30,31]. The plane-wave basis cutoff energy was set to  $283.0\text{ eV}$ .  $\Gamma$ -centered  $k$  points were used for the first Brillouin-zone sampling with a spacing of  $0.03\text{ \AA}^{-1}$ . The structures were optimized until the forces on atoms were less than  $5\text{ meV \AA}^{-1}$ . The pressure was derived by fitting the total energy dependence on the volume with the Murnaghan equation [32]. The phonon dispersion was carried out using the finite displacement method with VASP and the PHONOPY code [33], and a supercell with all the lattice dimension larger than  $10.0\text{ \AA}$  was employed to calculate the phonon spectra.

### III. RESULTS AND DISCUSSION

#### A. Properties of $\text{HfTe}_5$ at ambient pressure

Long ribbon-shaped  $\text{HfTe}_5$  crystals extended along the crystallographic  $a$  axis were used for the study. The EDXS analysis confirms that the single crystals are homogeneous and that the atomic ratio of elements is  $\text{Hf} : \text{Te} = 1 : 4.97(2)$ . The SXRD demonstrates that our  $\text{HfTe}_5$  samples adopt the  $Cmcm$  structure with lattice parameters  $a = 3.974(1)\text{ \AA}$ ,  $b = 14.481(2)\text{ \AA}$ , and  $c = 13.720(2)\text{ \AA}$ , in good agreement with previously reported structural data [34]. The crystal structure of  $\text{HfTe}_5$  is shown in Figs. 1(a) and 1(b). The  $\text{HfTe}_3$  prisms and the zigzag chains are connected through the apical Te atoms, and the Te-Te bond length between two chains is longer than that in the zigzag chain. Each  $\text{HfTe}_5$  layer is nominally charge neutral, and the interlayer distance (along the  $b$  axis) is quite large (about  $7.24\text{ \AA}$ ), suggesting a weak interlayer coupling, presumably of van der Waals type.

Interestingly, the specific heat of  $\text{HfTe}_5$  in a representation  $C_P/T$  vs  $T^2$  below  $T \approx 10\text{ K}$  [Fig. 1(c), inset] does not follow a linear relationship but shows a peculiar negative curvature. In that temperature range, a negative deviation from the Debye  $T^3$  behavior can only be explained by low-dimensional lattice vibrations. In an earlier investigation [35] for higher temperatures (6–20 K), a stronger deviation from the Debye

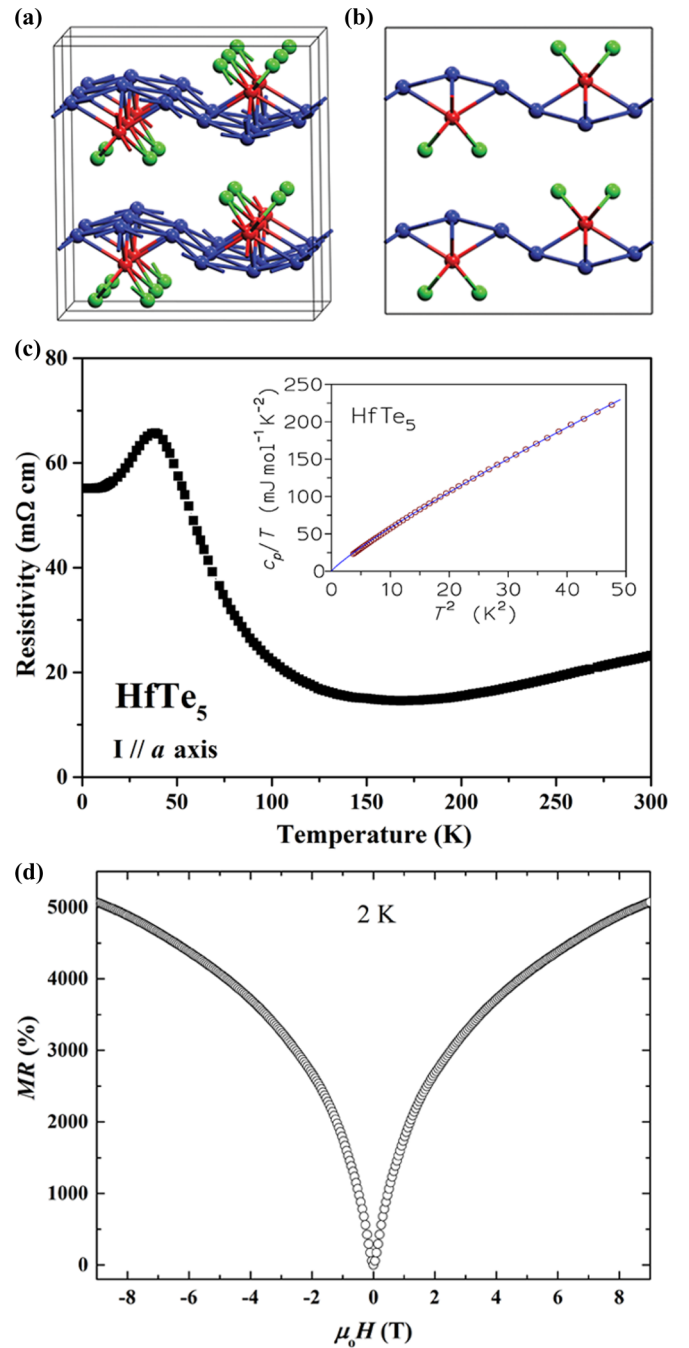


FIG. 1. Crystal structure and electrical and thermal properties of  $\text{HfTe}_5$  at ambient pressure. (a) Crystal structure of  $\text{HfTe}_5$  with  $Cmcm$  space group. The red spheres represent Hf atoms, and both green and blue spheres represent Te atoms at different crystallographic positions. (b) Side view of the  $\text{HfTe}_5$  crystal structure. The  $\text{HfTe}_3$  chains that run along the  $a$  axis are linked via zigzag chains of Te atoms. (c) Temperature-dependent resistivity of  $\text{HfTe}_5$  along the  $a$  axis. A large resistivity anomaly appears at around  $40\text{ K}$ . Inset: Specific heat capacity of  $\text{HfTe}_5$  crystals in the representation  $C_P/T$  vs  $T^2$ . (d) Magnetoresistance (MR) of  $\text{HfTe}_5$  at a temperature of  $2\text{ K}$  and in a maximum field of  $9\text{ T}$  with current and field along  $[100]$  and  $[010]$ , respectively.

theory for 3D materials was observed. The authors of Ref. [35] concluded that for  $\text{ZrTe}_5$  and  $\text{HfTe}_5$  the effective dimension

is between one and two. In our data, in the temperature range 1.9–6.9 K, a relationship  $C_P(T) = \gamma T + \beta' T^\alpha$  with  $\gamma = 0$  and  $\alpha \approx 2.7$  is followed. Thus, the deviations from 3D behavior are less severe, and HfTe<sub>5</sub> may at best be described as showing indications of a quasi-two-dimensional (2D) anisotropy. No significant contribution linear in  $T$  to  $C_P(T)$  is observed, indicating a negligible concentration (or the absence) of conduction electrons in HfTe<sub>5</sub> at ambient pressure.

Figure 1(c) shows the temperature dependence of the electrical resistivity in the chain ( $a$  axis) direction for a HfTe<sub>5</sub> single crystal at ambient pressure. The curve displays a pronounced anomalous peak near 40 K, in agreement with published data [14,15,36]. A similar resistive anomaly is observed in ZrTe<sub>5</sub> [13,14]. This anomaly in pentatellurides is

likely associated with peculiarities of their electronic structure, although the origin still remains elusive [37–39]. Similarities in structure between the pentatellurides and other chalcogenides strongly suggested the formation of a CDW as the origin of the resistivity anomalies. However, a search for direct evidence of CDWs in pentatellurides failed to demonstrate them [38]. Very recently, Zhao *et al.* reported that a 3D topological Dirac semimetal state emerges at temperatures around the resistivity peak, which they considered to indicate the topological quantum phase transition between two distinct weak and strong TI phases in HfTe<sub>5</sub> [40]. By approaching the topological critical point, the bulk band gap goes to zero, thereby giving rise to a pronounced resistivity peak. Our HfTe<sub>5</sub> crystals, in addition, display a quite large unsaturated magnetoresistance of 5100% at  $T = 2$  K in a magnetic field

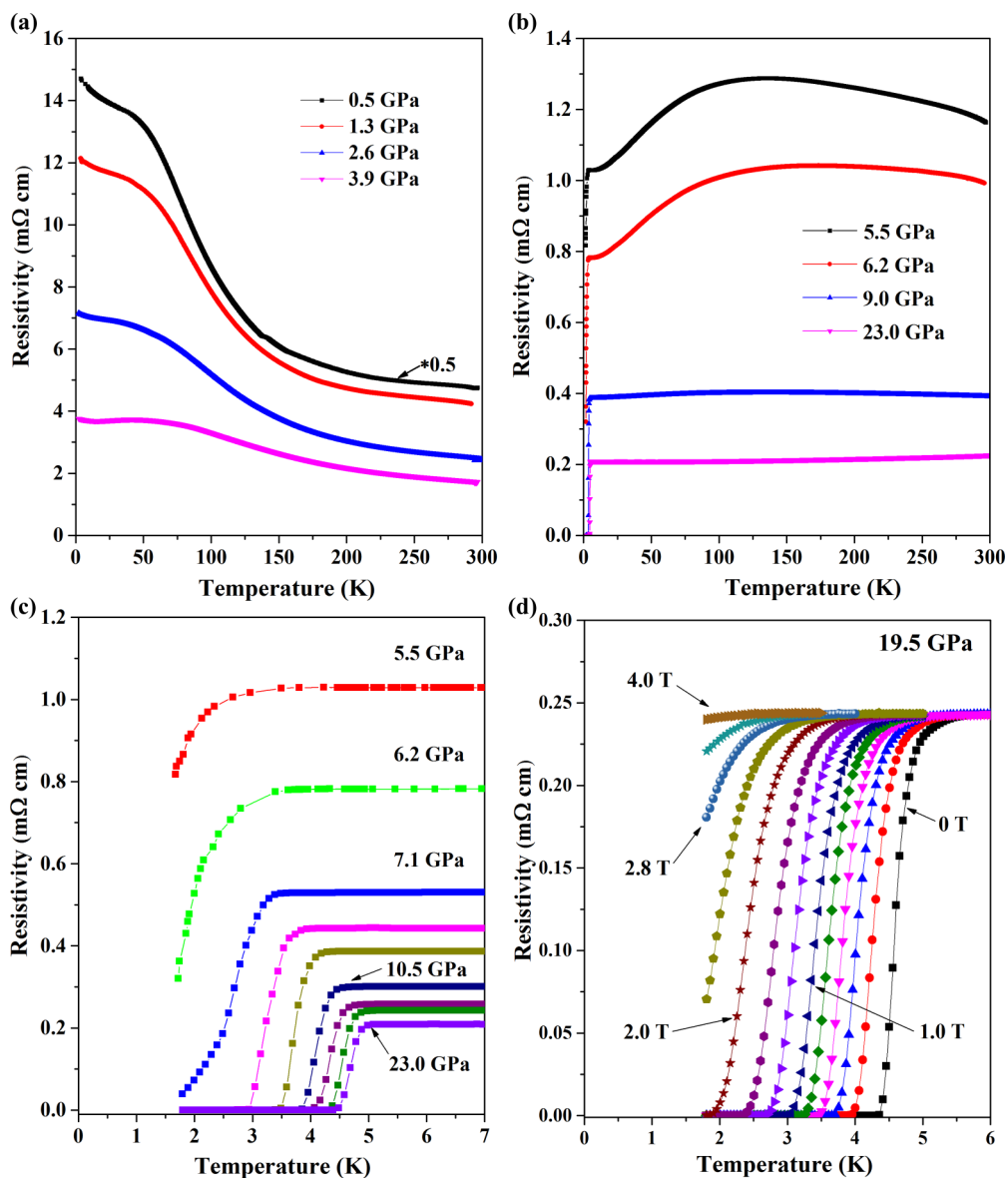


FIG. 2. Evolution of superconductivity as a function of pressure. Plots of electrical resistivity as function of temperature for  $P < 5$  GPa (a) and for  $P > 5$  GPa (b). At  $P = 5.5$  GPa and 6.2 GPa, superconductivity is observed although the normal state still exhibits the resistivity anomaly. (c) shows the electrical resistivity drop and zero-resistance behavior at low temperatures. The superconducting critical temperature  $T_c$  increases with increasing pressure, the maximum  $T_c = 4.8$  K is observed at 20 GPa. (d) Temperature dependence of resistivity under various magnetic fields up to  $\mu_0 H = 4$  T at 19.5 GPa.

of 9 T, as shown in Fig. 1(d). A large anisotropy in the electrical transport is present, which is typical for layered transition-metal chalcogenides [41].

## B. Measurements at high pressure

The resistivity anomaly in  $\text{HfTe}_5$ , even if its nature remains elusive, indicates that  $\text{HfTe}_5$  is located in the vicinity of an electronic instability. It is well known that SC often appears in compounds that are close to a structural, magnetic, or electronic instability. In this respect, pressure can effectively modify lattice structures and influence the corresponding electronic states in a systematic fashion. Hence, the electronic transport of  $\text{HfTe}_5$  has been studied as function of temperature at different pressures ( $P$ ).

Figure 2(a) shows the evolution of temperature dependence of electrical resistivity  $\rho(T)$  for pressures up to 42 GPa. For  $P < 5$  GPa,  $\rho(T)$  displays a semiconductinglike behavior similar to that observed at ambient pressure, albeit with a broadened and less pronounced anomaly. With increasing  $P$ , the temperature of the resistivity anomaly increases to  $\approx 110$  K at  $P \approx 5.0$  GPa but then seems to shift back toward lower temperatures at a further pressure increase. A similar pressure dependence of the resistivity anomaly is observed for  $\text{ZrTe}_5$  [22]. This obviously common pressure behavior of the two pentatellurides is different from that of chalcogenides exhibiting a CDW (CDW transitions are typically suppressed by application of pressure) [42].

Surprisingly, the onset of SC is observed at  $T_c = 1.8$  K as  $P$  increases above 5 GPa. At this pressure, the normal state still exhibits a pronounced resistivity anomaly at  $\approx 90$  K, as seen in Fig. 2(b). This behavior is different from what is observed in the sister compound  $\text{ZrTe}_5$ , where the SC phase emerges immediately when the peak anomaly disappears at a possible quantum critical point. With further increasing  $P$ , the resistivity anomaly is suppressed further, and for  $P > 9$  GPa the temperature dependence of  $\rho(T)$  changes to that of a normal metal. The critical temperature of SC,  $T_c$ , gradually increases with  $P$ , and the maximum  $T_c$  of 4.8 K is attained at

$P \approx 20$  GPa, as shown in Fig. 2(c). Beyond this pressure,  $T_c$  decreases very slowly and persists with  $T_c = 4.5$  K up to the highest attained pressure of 42 GPa.

The pressure evolution of  $T_c$  in  $\text{HfTe}_5$  is very similar to that of the superconducting phase I (SC-I) of  $\text{ZrTe}_5$  [22]. In contrast, we do not observe any indication of a second superconducting phase analogous to the SC-II phase in  $\text{ZrTe}_5$  [22]. Considering the close similarities in ambient-pressure properties and the pressure-driven behavior of both pentatellurides, it might be supposed that the SC-II phase in  $\text{ZrTe}_2$  is rather a metastable state characteristic only for this compound. The negligible variation of  $T_c$  over a very large range of pressure observed for both pentatellurides is highly unusual; however, a similar effect was observed for the pressure-induced SC in some topologically nontrivial systems such as  $\text{Bi}_2\text{Se}_3$  [43] and  $\text{BiTeCl}$  [44].

The appearance of SC in  $\text{HfTe}_5$  is further corroborated by the resistivity data in applied magnetic fields. As seen from Fig. 2(d), the SC transition gradually shifts toward lower temperatures with increasing magnetic fields. At  $\mu_0 H = 3$  T, the transition could not be observed above 1.8 K. The upper critical field,  $H_{c2}$ , is determined using the 90% points on the resistive transition curves. The initial slope  $d\mu_0 H_{c2}/dT$  at  $T_c$  is  $-1.08$  T K $^{-1}$ . A simple estimate using the conventional one-band Werthamer-Helfand-Hohenberg (WHH) approximation without considering the Pauli spin-paramagnetism effect and spin-orbit interaction [45],  $H_{c2}(0) = -0.693 T_c \times (dH_{c2}/dT)$  with  $\mu_0 H_{c2}$  in Tesla and  $T$  in Kelvin, yielded a value of 3.6 T. We also tried to use the Ginzburg-Landau formula to fit the data,

$$H_{c2}(T) = \frac{H_{c2}(0)(1-t^2)}{1+t^2},$$

where  $t$  is the reduced temperature  $T/T_c$ . The resulting upper critical field  $\mu_0 H_{c2}(0) = 4.5$  T. These  $H_{c2}$  values are obviously higher than that obtained in the sister compound  $\text{ZrTe}_5$  [22]. According to the relationship between  $H_{c2}$  and the Ginzburg-Landau coherence length  $\xi_{\text{GL}}$ , namely,  $H_{c2} = \Phi_0/(2\pi\xi^2)$ ,

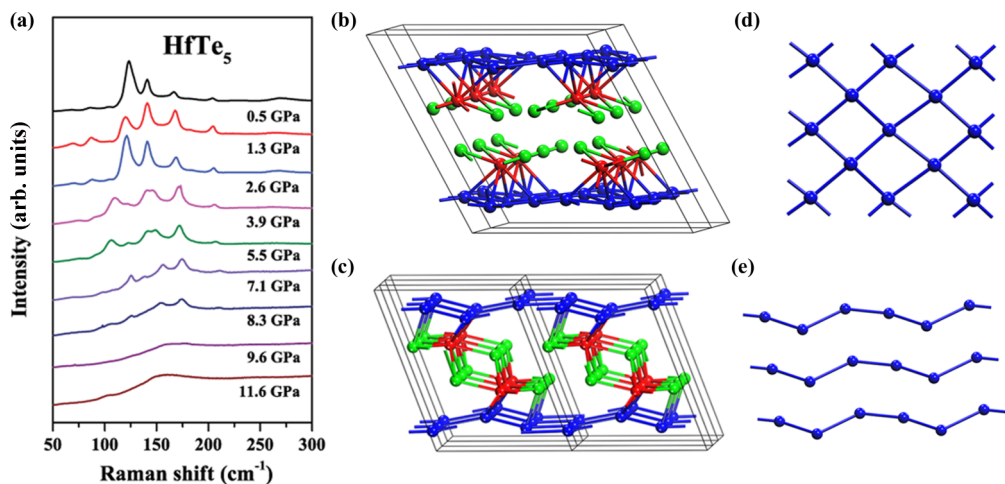


FIG. 3. Raman spectroscopy of  $\text{HfTe}_5$  and possible crystal structure under high pressure. (a) Pressure-dependent Raman spectroscopic signals for  $\text{HfTe}_5$  at room temperature. (b), (c) Crystal structures of the  $C2/m$  and  $P\bar{1}$  phases. The red spheres represent Hf atoms, and both green and blue spheres represent Te atoms with different positions. (d) and (e) show the Te layers of the  $C2/m$  phase and the Te chains of the  $P\bar{1}$  phase.

where  $\Phi_0 = 2.07 \times 10^{-15}$  Wb is the flux quantum, the derived  $\xi_{\text{GL}}(0)$  is 8.5 nm. It is also worth noting that our estimated value of  $H_{c2}(0)$  is well below the Pauli-Clogston limit.

The previously described changes of the electronic properties of HfTe<sub>5</sub> at high pressures might be associated with pressure-induced structural transitions. Raman spectroscopy is a powerful tool to probe changes in the crystal lattice, and thus, our pressure-dependent electronic transport measurements of HfTe<sub>5</sub> were accompanied by such spectroscopic studies. Figure 3(a) shows the Raman spectra of HfTe<sub>5</sub> at various pressures. The modes observed at the lowest experimental pressure of 0.5 GPa are similar to those reported previously at ambient pressure [46,47]. With increasing pressure, the profile of the spectra remains similar to that at ambient pressure, whereas the observed modes shift toward higher frequencies, thus showing the normal pressure behavior. When  $P$  approaches 4–5 GPa, the splitting of observed vibrational modes indicates the structural phase transition to high-pressure phase II. It should be noted that the SC is observed beyond this pressure. An abrupt disappearance of Raman peaks for  $P > 9$  GPa indicates the next structural phase transition to phase III. The absence of Raman peaks is consistent with the normal metallic state observed in our resistance measurements in this phase above 9 GPa. In sum, the Raman study provides evidence for two pressure-induced structural phase transitions.

### C. Phase stabilities and electronic structure

Similarly, two structural phase transitions, from *Cmcm* to *C2/m* and to *P̄1*, have been reported in recent high-pressure studies of ZrTe<sub>5</sub> [22]. Considering the close similarities between ambient-pressure structure and high-pressure behavior of the electronic properties of the two compounds, it is natural to suppose that HfTe<sub>5</sub> adopts at high pressure the same crystal structures as ZrTe<sub>5</sub>. The DFT calculations of phase stabilities of HfTe<sub>5</sub> in these structures at high pressure confirm our suggestion. The enthalpy difference curves for the three phases are shown in Fig. 4. The enthalpy,  $H$ , of a given phase is evaluated to identify the energetically favored ground state for

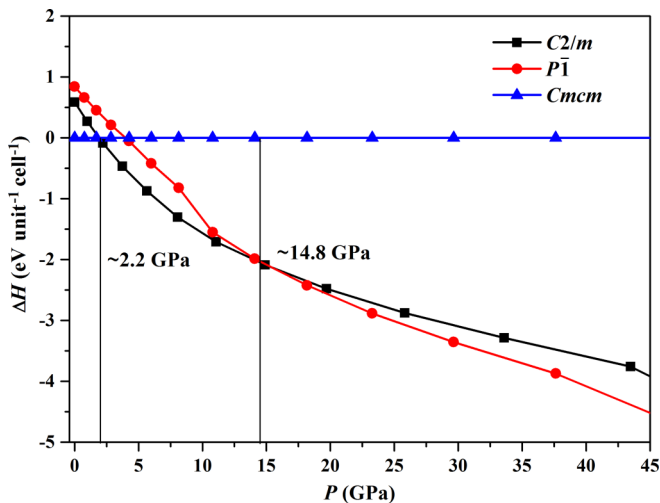


FIG. 4. Enthalpy curves (relative to the *Cmcm* structure) of various structures of HfTe<sub>5</sub> as function of pressure. Enthalpies are given per unit cell (Hf<sub>2</sub>Te<sub>10</sub>).

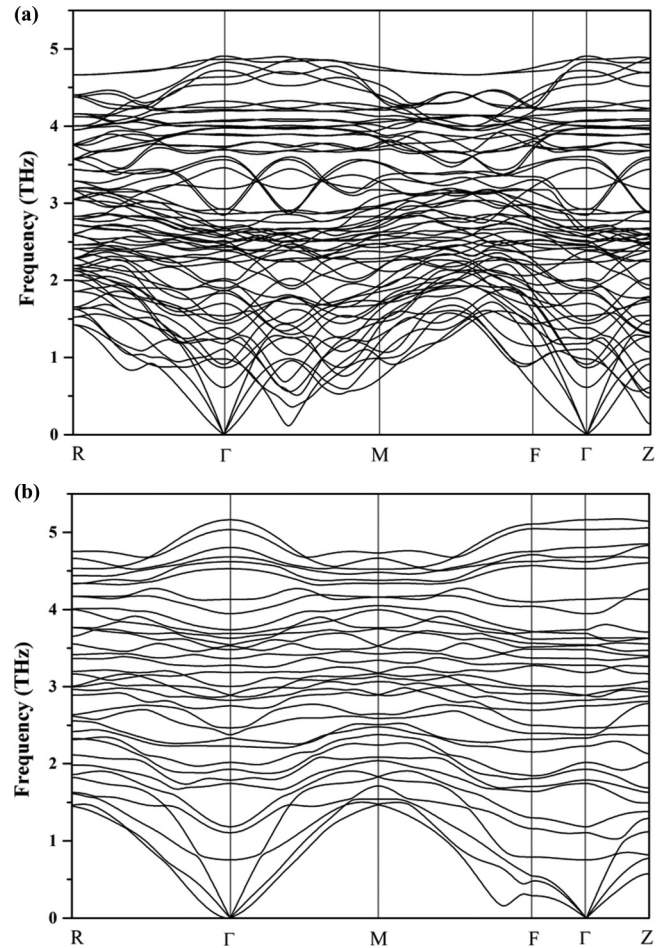


FIG. 5. The calculated phonon spectra of the *C2/m* and *P̄1* phases of HfTe<sub>5</sub>. The phonon spectra of the high-pressure phases demonstrate that both the *C2/m* (a) and *P̄1* (b) phases are stable.

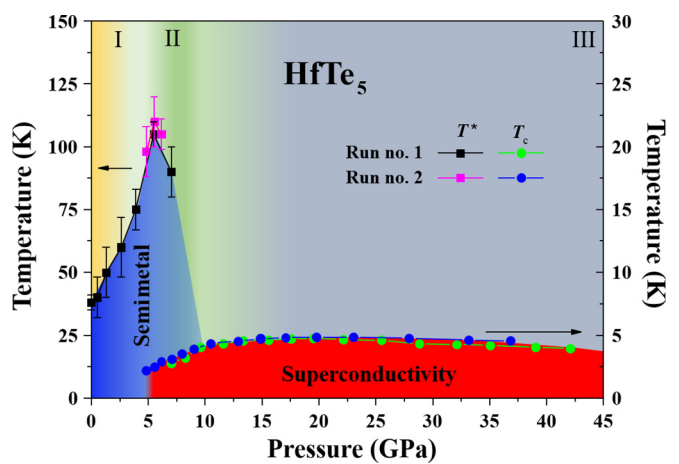


FIG. 6. Electronic phase diagram of HfTe<sub>5</sub>. The black and magenta squares denote  $T^*$ , the peak temperature of the electrical resistivity anomaly defined as the temperature of the discontinuity in the resistivity derivative. The green and blue circles represent  $T_c$  extracted from different runs of electrical resistivity measurements. Colored areas are a guide to the eye indicating the distinct phases.

a finite pressure by  $H = E_{\text{tot}} + PV$ , where  $E_{\text{tot}}$  is the total energy of the system and  $V$  is the volume of a unit cell. The enthalpy-pressure curves indicate that the *Cmcm* structure is indeed the most stable one at ambient pressure, which agrees well with the experiment. In the pressure range from about 2.2 to 14.8 GPa, the orthorhombic *C2/m* phase has the lowest enthalpy, but for higher pressure the *P̄1* phase takes over the ground state. The corresponding transition pressures are in good agreement with our Raman spectroscopy results. Since the *Cmcm* structure is experimentally verified for ambient pressure, we further verified the stabilities of the other two high-pressure phases by the phonon spectrum calculations (see Fig. 5), confirming that both *C2/m* and *P̄1* phases are dynamically stable. The crystal structures of the *C2/m* and *P̄1* phases are shown in Figs. 3(b) and 3(c). The *Cmcm* and *C2/m* phases are similar in structure, in which a distorted square lattice of Te atoms exists. The Te layer is strongly corrugated in the *Cmcm* phase while it is relatively flat in the *C2/m*

phase. By contrast, the corresponding Te layer turns into a 1D chainlike structure in the *P̄1* phase with the lowest symmetry [Figs. 3(d) and 3(e)].

The high-pressure experiments have been repeated on different samples with good reproducibility of the observed transition temperatures. All of the characteristic temperatures from our experiments, the peak temperature of the electrical resistivity anomaly ( $T^*$ ), and the superconducting transition temperature ( $T_c$ ), are summarized in a  $T$ - $P$  phase diagram in Fig. 6. According to Raman spectroscopic data, there are two high-pressure phases (*C2/m*, phase II and *P̄1*, phase III) in addition to the ambient-pressure phase (*Cmcm*, phase I). With increasing pressure, the peak temperature of the resistivity initially increases to around 110 K and then decreases abruptly in phase II. The SC appears with phase II, while the resistivity anomaly is still present at a higher temperature. In phase III, a metallic normal state is reached. The SC  $T_c$  changes slowly with a maximum critical temperature of 4.8 K at  $P \approx 20$  GPa,

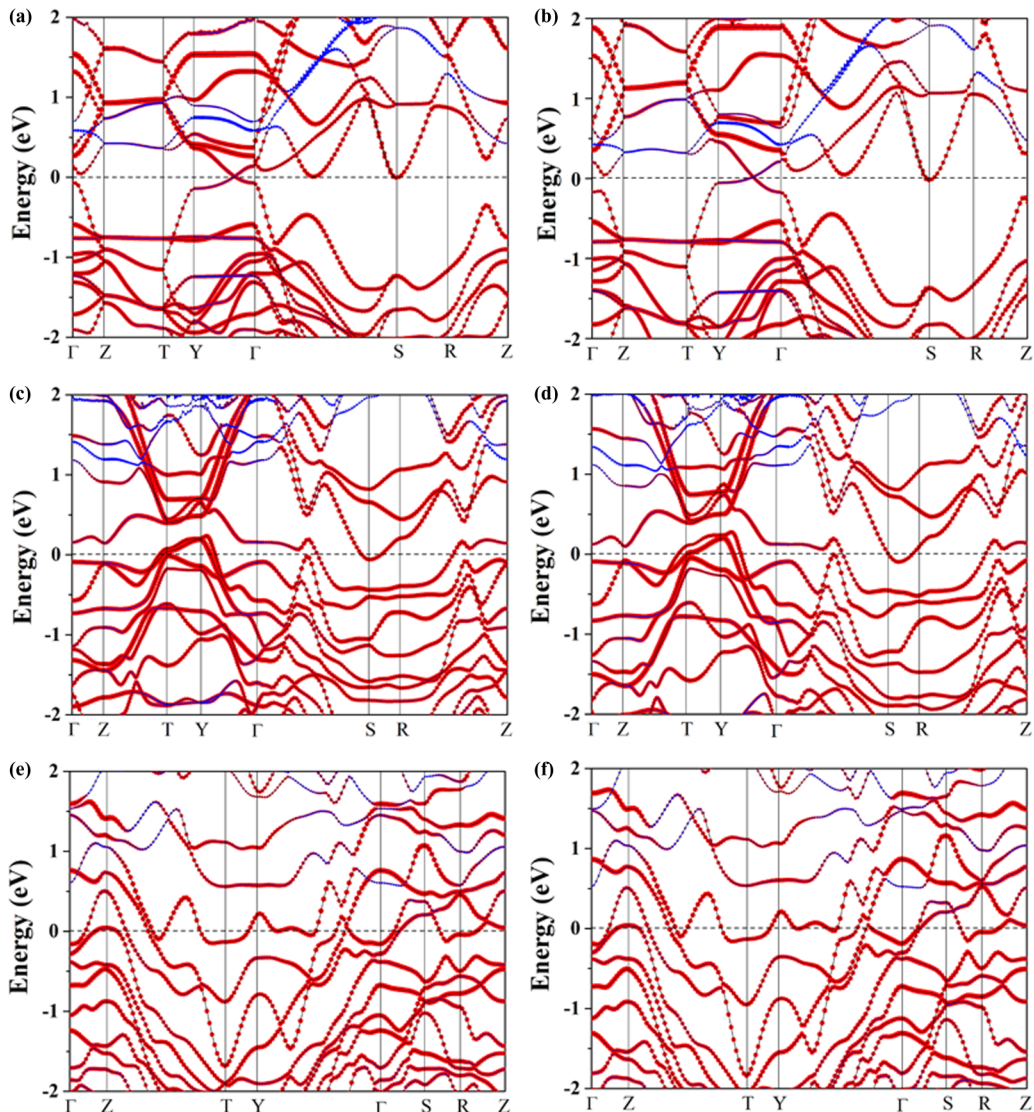


FIG. 7. Electronic band structure for  $\text{HfTe}_5$  as function of pressure. The DFT calculated electronic band structures of  $\text{HfTe}_5$  at 0 GPa (a) and 2.2 GPa (b) in *Cmcm* phase, 2.3 GPa (c) and 8.1 GPa (d) in *C2/m* phase, 10.8 GPa (e) and 17.5 GPa (f) in *P̄1* phase. (a)-(f) The size of red filled circles (blue filled triangles) represents the fraction of Te 5p (Hf 5d) states. [ $\Gamma$ : (0, 0, 0, 0); Z: (0, 0, 0,  $\pi/a$ ); T: ( $\pi/a$ ,  $\pi/a$ ,  $\pi/a$ ); Y: ( $\pi/a$ ,  $\pi/a$ , 0, 0); S: (0, 0,  $\pi/a$ , 0, 0); R: (0, 0,  $\pi/a$ ,  $\pi/a$ )].

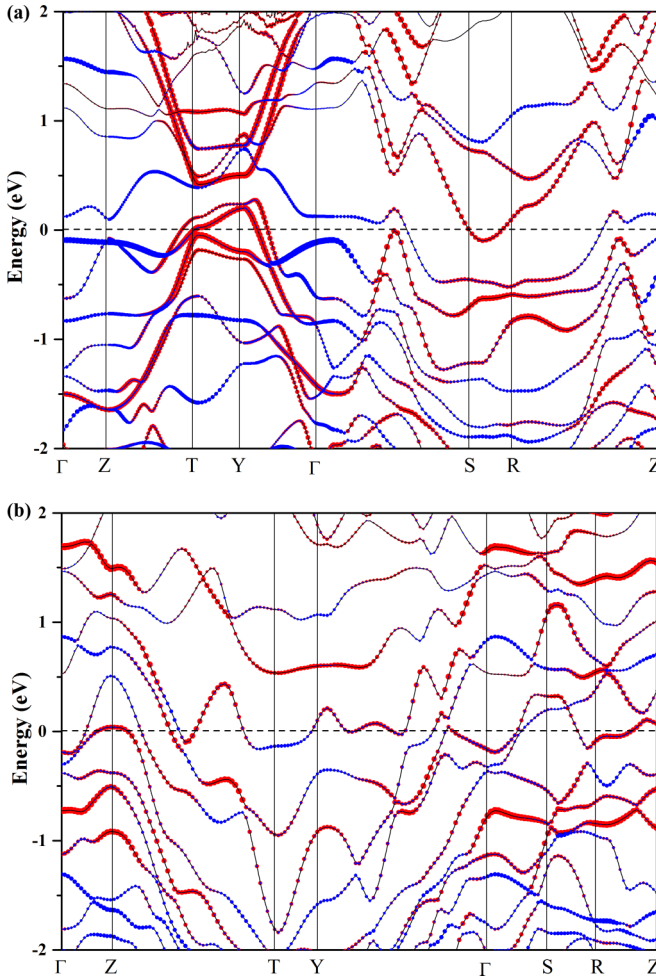


FIG. 8. Electronic band structure for  $\text{HfTe}_5$  as function of pressure calculated by DFT at 8.1 GPa in the  $C2/m$  phase (a) and at 17.5 GPa in the  $P\bar{1}$  phase (b). The size of the red spheres represents the fraction of the in-layer (in-chain) Te 5p states in the  $C2/m$  ( $P\bar{1}$ ) phase, while the size of blue filled triangles represents the fraction of the out-of-layer (out-of-chain) Te 5p states in  $C2/m$  ( $P\bar{1}$ ) phase.

and SC persists up to the highest pressure of 42 GPa with  $T_c = 4.5 \text{ K}$ .

The electronic band structure and density of states (DOS) can help to further understand the properties of  $\text{HfTe}_5$ . As shown in Figs. 7(a) and 7(b), the  $Cmcm$  phase is semimetallic, in agreement with our resistivity and specific heat results. Here Hf-5d and Te-5p states exhibit a band anticrossing near the Fermi energy  $E_F$ , which is consistent with the observed band inversion in a previous calculation [19]. However, the other two high-pressure phases are metallic and display large DOS at the Fermi energy  $E_F$  [see Figs. 7(c–f)]. Herein the states at  $E_F$  are mainly contributed by the Te-5p states with negligible contribution of Hf-5d states. In the  $C2/m$  phase, the in-layer Te-5p states are dominant in the DOS at  $E_F$  compared to those of the rest Te atoms. Similarly, in the  $P\bar{1}$  phase, the in-chain Te-5p states are dominant, as shown in Fig. 8. We note that the abrupt increase of DOS at the transition points shown in Fig. 9 is due to the fact that we simulated only the pressure behavior of neighboring phases of the transition rather than the real continuous structural deformation from

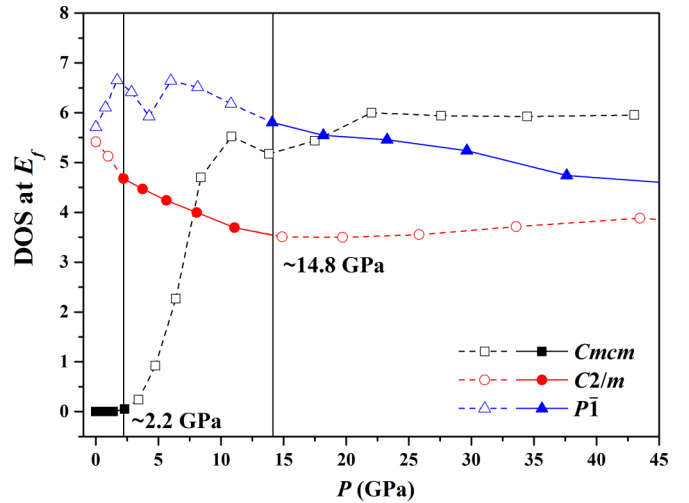


FIG. 9. The evolution of the electronic density of states (DOS) at the Fermi level with the increase of pressure for  $\text{HfTe}_5$ .

one phase to the other in experiment. However, we can still estimate the general trend of DOS: It increases up to the pressure region when the II-III transition happens and then decreases slowly, which agrees roughly with the  $T_c$  in our SC phase diagram. With increasing pressure, the DOS increases suddenly when  $\text{HfTe}_5$  transforms into the intermediate phase II structure. At this pressure, SC rises suddenly above our experimental low-temperature limit. At the second transition (II-III), the DOS and  $T_c$  further increase simultaneously. In phase III, DOS and  $T_c$  decrease simultaneously with increasing pressure. Considering that the SC occurs among the electronic states at the Fermi energy, the SC of the  $\text{HfTe}_5$  high-pressure phases may be hosted in different channels: inside the Te layers for the  $C2/m$  phase and among the Te chains for the  $P\bar{1}$  phase. This connection of SC to specific structural subunits of  $\text{HfTe}_5$  resembles the situation in the 2D cuprates ( $\text{CuO}_2$  planes) [48] and iron-pnictides ( $\text{Fe}_2\text{As}_2$  layers) [49] on the one hand, and in some quasi-1D organic superconductors [as  $(\text{TMTSF})_2X$ ] [50] on the other hand. It may lead to interesting quasi-2D and quasi-1D superconducting properties of  $\text{HfTe}_5$  under pressure.

#### IV. CONCLUSION

In summary, metallicity and SC were successfully induced in the semimetal  $\text{HfTe}_5$  by application of high pressure. The appearance of SC is accompanied by the suppression of the resistivity anomaly as well as by a structural phase transition. Thus, the resistivity anomaly, a nontrivial topological state, and SC were all observed in  $\text{HfTe}_5$ , all contributing to the highly interesting physics seen in this transition-metal pentatelluride.

*Note added.* After we submitted this paper, we learned that similar work was carried out independently by another group and published as an e-print (arXiv: 1603.00514) [51]. Most of the data in that paper are consistent with our results.

## ACKNOWLEDGMENTS

Y. Qi acknowledges financial support from the Alexander von Humboldt Foundation. This work was financially supported by the Deutsche Forschungsgemeinschaft (DFG;

Project No. EB 518/1-1 of DFG-SPP 1666 “Topological Insulators”) and by the European Research Council (ERC Advanced Grant No. 291472, “Idea Heusler”).

- [1] F. Hulliger, in *Structure and Bonding* (Springer, Berlin, 1968), Vol. 4, pp. 83–229.
- [2] F. Hulliger, Structural Chemistry of Layer-Type Phases, in *Physics and Chemistry of Materials with Layered Structures*, edited by F. Lévy (Springer, Netherlands, 1976), Vol. 5.
- [3] J. A. Wilson and A. D. Yoffe, *Adv. Phys.* **18**, 193 (1969).
- [4] M. N. Ali, J. Xiong, S. Flynn, J. Tao, Q. D. Gibson, L. M. Schoop, T. Liang, N. Haldolaarachchige, M. Hirschberger, N. P. Ong, and R. J. Cava, *Nature* **514**, 205 (2014).
- [5] D. H. Keum, S. Cho, J. H. Kim, D. H. Choe, H. J. Sung, M. Kan, H. Kang, J. Y. Hwang, S. W. Kim, H. Yang, K. J. Chang, and Y. H. Lee, *Nat. Phys.* **11**, 482 (2015).
- [6] A. A. Soluyanov, D. Gresch, Z. Wang, Q. Wu, M. Troyer, X. Dai, and B. A. Bernevig, *Nature* **527**, 495 (2015).
- [7] Y. Sun, S.-C. Wu, M. N. Ali, C. Felser, and B. Yan, *Phys. Rev. B* **92**, 161107 (2015).
- [8] X. Qian, J. Liu, L. Fu, and J. Li, *Science* **346**, 1344 (2014).
- [9] X. Xu, W. Yao, D. Xiao, and T. F. Heinz, *Nat. Phys.* **10**, 343 (2014).
- [10] Y. J. Zhang, T. Oka, R. Suzuki, J. T. Ye, and Y. Iwasa, *Science* **344**, 725 (2014).
- [11] S. Takahashi, T. Sambongi, J. W. Brill, and W. Roark, *Solid State Commun.* **49**, 1031 (1984).
- [12] X. Zhu, H. Lei, and C. Petrovic, *Phys. Rev. Lett.* **106**, 246404 (2011).
- [13] S. Okada, T. Sambongi, and M. Ido, *J. Phys. Soc. Jpn.* **49**, 839 (1980).
- [14] E. F. Skelton, T. J. Wieting, S. A. Wolf, W. W. Fuller, D. U. Gubser, T. L. Francavilla, and F. Lévy, *Solid State Commun.* **42**, 1 (1982).
- [15] M. Izumi, K. Uchinokura, and E. Matsuura, *Solid State Commun.* **37**, 641 (1981).
- [16] T. E. Jones, W. W. Fuller, T. J. Wieting, and F. Levy, *Solid State Commun.* **42**, 793 (1982).
- [17] M. Izumi, T. Nakayama, K. Uchinokura, S. Harada, R. Yoshizaki, and E. Matsuura, *J. Physics C: Solid State Phys.* **20**, 3691 (1987).
- [18] G. N. Kamm, D. J. Gillespie, A. C. Ehrlich, D. L. Peebles, and F. Levy, *Phys. Rev. B* **35**, 1223 (1987).
- [19] H. Weng, X. Dai, and Z. Fang, *Phys. Rev. X* **4**, 011002 (2014).
- [20] Q. Li, D. E. Kharzeev, C. Zhang, Y. Huang, I. Pletikosić, A. V. Fedorov, R. D. Zhong, J. A. Schneeloch, G. D. Gu, and T. Valla, *Nat. Phys.* **12**, 550 (2016).
- [21] R. Y. Chen, Z. G. Chen, X. Y. Song, J. A. Schneeloch, G. D. Gu, F. Wang, and N. L. Wang, *Phys. Rev. Lett.* **115**, 176404 (2015).
- [22] Y. H. Zhou, J. Wu, W. Ning, N. Li, Y. Du, X. Chen, R. Zhang, Z. Chi, X. Wang, X. Zhu, P. Lu, C. Ji, X. Wan, Z. Yang, J. Sun, W. Yang, M. Tian, Y. Zhang, and H. Mao, *PNAS* **113**, 2904 (2015).
- [23] S. Medvedev, T. M. McQueen, I. A. Troyan, T. Palasyuk, M. I. Eremets, R. J. Cava, S. Naghavi, F. Casper, V. Ksenofontov, G. Wortmann, and C. Felser, *Nat. Mater.* **8**, 630 (2009).
- [24] Y. Qi, P. G. Naumov, M. N. Ali, C. R. Rajamathi, W. Schnelle, O. Barkalov, M. Hanfland, S. C. Wu, C. Shekhar, Y. Sun, V. Süß, M. Schmidt, U. Schwarz, E. Pippel, P. Werner, R. Hillebrand, T. Förster, E. Kampert, S. Parkin, R. J. Cava *et al.*, *Nat. Commun.* **7**, 11038 (2016).
- [25] H. K. Mao, J. Xu, and P. M. Bell, *J. Geophysical Res.: Solid Earth* **91**, 4673 (1986).
- [26] G. Kresse and J. Furthmüller, *Phys. Rev. B* **54**, 11169 (1996).
- [27] P. E. Blöchl, *Phys. Rev. B* **50**, 17953 (1994).
- [28] G. Kresse and D. Joubert, *Phys. Rev. B* **59**, 1758 (1999).
- [29] J. P. Perdew, K. Burke, and M. Ernzerhof, *Phys. Rev. Lett.* **77**, 3865 (1996).
- [30] S. Grimme, J. Antony, S. Ehrlich, and H. Krieg, *J. Chem. Phys.* **132**, 154104 (2010).
- [31] S. Grimme, S. Ehrlich, and L. Goerigk, *J. Computational Chem.* **32**, 1456 (2011).
- [32] F. D. Murnaghan, *Proc. Natl. Acad. Sci. USA* **30**, 244 (1944).
- [33] A. Togo, F. Oba, and I. Tanaka, *Phys. Rev. B* **78**, 134106 (2008).
- [34] H. Fjellvåg and A. Kjekshus, *Solid State Commun.* **60**, 91 (1986).
- [35] R. Shaviv, E. F. Westrum, Jr., H. Fjellvåg, and A. Kjekshus, *J. Solid State Chem.* **81**, 103 (1989).
- [36] H. Wang, C.-K. Li, H. Liu, J. Yan, J. Wang, J. Liu, Z. Lin, Y. Li, Y. Wang, L. Li, D. Mandrus, X. C. Xie, J. Feng, and J. Wang, *Phys. Rev. B* **93**, 165127 (2016).
- [37] F. J. DiSalvo, R. M. Fleming, and J. V. Waszczak, *Phys. Rev. B* **24**, 2935 (1981).
- [38] S. Okada, T. Sambongi, M. Ido, Y. Tazuke, R. Aoki, and O. Fujita, *J. Phys. Soc. Jpn.* **51**, 460 (1982).
- [39] D. N. McIlroy, S. Moore, Z. Daqing, J. Wharton, B. Kempton, R. Littleton, M. Wilson, T. M. Tritt, and C. G. Olson, *J. Phys.: Condensed Matter* **16**, L359 (2004).
- [40] L. X. Zhao, X. C. Huang, Y. J. Long, D. Chen, H. Liang, Z. H. Yang, M. Q. Xue, Z. A. Ren, H. M. Weng, Z. Fang, X. Dai, G. F. Chen, [arXiv:1512.07360](https://arxiv.org/abs/1512.07360).
- [41] N. Kumar, C. Shekhar, H. Borrmann, and C. Felser, (unpublished).
- [42] A. F. Kusmartseva, B. Sipos, H. Berger, L. Forró, and E. Tutiš, *Phys. Rev. Lett.* **103**, 236401 (2009).
- [43] K. Kirshenbaum, P. S. Syers, A. P. Hope, N. P. Butch, J. R. Jeffries, S. T. Weir, J. J. Hamlin, M. B. Maple, Y. K. Vohra, and J. Paglione, *Phys. Rev. Lett.* **111**, 087001 (2013).
- [44] J.-J. Ying, V. V. Struzhkin, Z.-Y. Cao, A. F. Goncharov, H.-K. Mao, F. Chen, X.-H. Chen, A. G. Gavriliuk, and X.-J. Chen, *Phys. Rev. B* **93**, 100504 (2016).
- [45] N. R. Werthamer, E. Helfand, and P. C. Hohenberg, *Phys. Rev.* **147**, 295 (1966).
- [46] I. Taguchi, A. Grisel, and F. Lévy, *Solid State Commun.* **45**, 541 (1983).

- [47] G. Landa, A. Zwick, R. Carles, M. A. Renucci, and A. Kjekshus, *Solid State Commun.* **50**, 297 (1984).
- [48] J. G. Bednorz and K. A. Müller, *Z. Physik B: Condensed Matter* **64**, 189 (1986).
- [49] Y. Kamihara, T. Watanabe, M. Hirano, and H. Hosono, *J. Am. Chem. Soc.* **130**, 3296 (2008).
- [50] D. Jérôme and H. J. Schulz, *Adv. Phys.* **31**, 299 (1982).
- [51] Y. Liu, Y. J. Long, L. X. Zhao, S. M. Nie, S. J. Zhang, Y. X. Weng, M. L. Jin, W. M. Li, Q. Q. Liu, Y. W. Long, R. C. Yu, X. L. Fen, Q. Li, H. M. Weng, X. Dai, Z. Fang, G. F. Chen, and C. Q. Jin, [arXiv:1603.00514](https://arxiv.org/abs/1603.00514).